


Time evolution of the Auger cascade for Kr $3d^95p$

Sigitas Kučas* and Valdas Jonauskas 

Institute of Theoretical Physics and Astronomy Vilnius University, Saulėtekio avenue 3, LT-10257 Vilnius, Lithuania

 (Received 20 December 2022; revised 28 July 2023; accepted 1 August 2023; published 22 August 2023)

The systematic theoretical study of the cascaded Auger decay following the $3d \rightarrow 5p$ excitation in Kr is presented. The origin of the Kr^{3+} ions in the cascade is explained by analyzing the influence of the correlation effects. The study shows that the time dependence of population for the Kr^+ ion resembles results for the Kr^{3+} ion obtained using ultrafast laser spectroscopy. It is demonstrated that different states of the Kr^+ and Kr^{2+} ions can contribute to the population of the Kr^{3+} ion observed in the probe-pulse experiments. Furthermore, the deeper states that could be reached by the probe laser pulse produce a peak shift for the population to the higher time delays in accordance with experimental observations for the higher pulse intensities.

DOI: [10.1103/PhysRevA.108.022810](https://doi.org/10.1103/PhysRevA.108.022810)

I. INTRODUCTION

Inner-shell vacancy produced in atoms or ions decays through a cascade of elementary processes with the emission of electrons from atomic systems in every step of the cascade leading to high ionization stages. The cascade ends when all produced states are below the ionization threshold of the corresponding ion. This process plays an important role in photoionized plasmas, which are observed in x-ray binaries [1,2] and active galactic nuclei [3–5]. The Auger cascade is one of the mechanisms defining charge state distribution in the photoionized plasma [6–8]. The photoionized plasmas are also produced using high power lasers and fast magnetic pinch machines [7,9,10]. Resonant excitations from the inner shells followed by the Auger cascades explain a considerable increase of the charge state in the x-ray multiphoton ionization [11]. What is more, the Auger electrons emitted in the cascade process following internal conversion or electron capture are exploited for cancer therapies [12–14]. The emission of many low-energy electrons produced by the Auger cascades is used in nanomedicine to increase the local radiation doses in the tumor region [15,16]. By this, the side effects accompanying the conventional treatment of cancer are minimized.

Real-time observation of electron or nuclear dynamics opened new possibilities for studies of ultrafast processes in atoms, molecules, and solid-state materials [17–19]. The pump-probe technique allowed one to observe the movement of the electron released into a continuum by initial laser pulse [20,21]. The probe pulses of the laser were also used to investigate excited intermediate states of the Auger cascade by interrupting the decay process [19,22,23]. The wavelength and intensity of the probing laser determine which intermediate states of the Auger cascade are triggered and which final states are populated.

Analysis of radiative and Auger spectra and ion yields produced by the Auger cascade demonstrated the complex

nature of the decay process and attracted the attention of researchers. Interpretation of the Auger cascades is a challenging problem since one has to deal with many radiative and Auger transitions, which can reach thousands or even millions of lines [24,25]. Furthermore, many-electron effects such as the correlation effects [26], multiple Auger transitions [27], shake transitions [28], and intermolecular Coulombic decay [29] can play a significant role in the relaxation process. The fundamental understanding of the cascades of the elementary processes is important for the further progress of theory and for providing ideas on how to control the behavior of such processes.

Previously, the Auger cascade following the $3d \rightarrow 5p$ excitation in krypton has been widely studied theoretically and experimentally [30–34]. Experimental ion yields produced in the decay process amount to 17% of Kr^+ , 73% of Kr^{2+} , and 10% of Kr^{3+} [34]. It was concluded that the Kr^{3+} ion is a result of the direct triple Auger transitions [34]. Besides, a comparison for integrated peak intensities suggested that the two-step Auger transitions account for $51 \pm 5\%$ of the Kr^{2+} ions. Therefore, the rest of the population received by the Kr^{2+} ions is a result of the double Auger transitions. On the other hand, the study of double and triple Auger transitions for the C^+ ion determined very low probabilities for an additional emission of electrons [27,35–37]. An advance in the ultrafast spectroscopy renewed interest for the investigation of the Auger cascade following the $3d \rightarrow 5p$ excitation in krypton [19,38,39]. New insights into the Auger cascade following the $3d \rightarrow 5p$ excitation from the ground $3d^{10}4s^24p^6$ configuration of the Kr atom were provided using transient absorption spectroscopy [19]. Previously, the multiconfiguration Dirac-Fock (MCDF) calculations were used to evaluate the Auger transition rates. What is more, these calculations included the shake transitions [19,39]. However, no theoretical studies for the ion yields and time evolution of the population for the produced ions were presented. Furthermore, the production of the Kr^{3+} ions was not explained.

The aim of our work is to study the Auger cascade following the $3d \rightarrow 5p$ excitation in the Kr atom. The main focus is

*Sigitas.Kucas@tfai.vu.lt

to evaluate the origin of the Kr^{3+} ions and present an analysis of time evolution for the population of the ions and their states. The other aim of the present work is to demonstrate that a proper treatment of the correlation effects is needed in the study of the cascaded Auger decay.

The rest of the paper is organized as follows. Section II presents a brief outline of the theoretical approach. In Sec. III, the obtained results are discussed. Finally, we end with the conclusions from the present investigation.

II. THEORETICAL APPROACH

Energy levels, radiative, and Auger transition probabilities are studied using flexible atomic code (FAC), where the Dirac-Fock-Slater approximation is implemented [40]. The investigation is made using the configuration-interaction (CI)

$$\bar{E}(K, K') = \frac{\sum_{\gamma\gamma'} [\langle \Phi(K\gamma) | H | \Phi(K\gamma) \rangle - \langle \Phi(K'\gamma') | H | \Phi(K'\gamma') \rangle] \langle \Phi(K\gamma) | H | \Phi(K'\gamma') \rangle^2}{\sum_{\gamma\gamma'} \langle \Phi(K\gamma) | H | \Phi(K'\gamma') \rangle^2}. \quad (2)$$

The admixed configurations are formed by incorporating single and double excitations from shells with the principal quantum numbers $n \geq 3$ to shells ranging from 4 to 7. The pseudorelativistic method [45] is used to obtain radial orbitals for the generated CIS configurations.

Auger cascade is studied from the levels of the $3d^9 5p$ configuration that is produced through the $3d \rightarrow 5p$ excitation by photon from the ground configuration of the Kr atom. Current analysis does not include population of the levels within the $3d^9 5p$ configuration through photoexcitation. It should be noted that the interference effects between direct photoionization and resonant excitation with subsequent Auger decay play a minor role at energies corresponding to the excitations to the $5p$ subshell of the Kr atom [46].

Population of level f produced by Auger transition from the level i is calculated using the following equation:

$$n_f = \sum_i n_i \frac{A_{if}^a}{\sum_m A_{im}^a}. \quad (3)$$

Here, n_l is the population of level l ($l = i, f$); A_{if}^a is a probability of Auger transition. On the other hand, configuration average transitions [47] were used previously to study the Auger cascades in Eu [48] and Xe [49]. The study for energy levels is more complex compared to the configuration average calculations since one configuration can have from tens to thousands of the energy levels. However, the level-to-level study is often required to provide more reliable results.

Time dependence of populations for levels is determined by solving the system of coupled rate equations:

$$\frac{dn_f(t)}{dt} = \sum_i n_i(t) A_{if}^a - n_f(t) \left(\sum_m A_{fm}^a \right). \quad (4)$$

Here, $n_f(t)$ is the population of level f at time t .

method. The configuration interaction strength (CIS) is utilized to generate the bases of admixed configurations [41–44]:

$$T(K, K') = \frac{\sum_{\gamma\gamma'} \langle \Phi(K\gamma) | H | \Phi(K'\gamma') \rangle^2}{\bar{E}(K, K')^2}. \quad (1)$$

By dividing this quantity by the statistical weight $g(K)$ of the studied configuration K , we can determine the average contribution of the admixed configuration K' to the expansion of the wave function for K . In Eq. (1), the summation is carried out across all states γ and γ' associated with the configurations K and K' , respectively. The quantity $\langle \Phi(K\gamma) | H | \Phi(K'\gamma') \rangle$ represents the interconfiguration matrix element of the two-electron electrostatic Hamiltonian. Additionally, $\bar{E}(K, K')$ denotes the average energy difference between the configurations:

III. RESULTS

The single-configuration approximation is not able to explain the production of the Kr^{3+} states (Fig. 1). This is one of the reasons why previous studies identified the production of the Kr^{3+} ions as a result of the triple Auger decay [34]. The $\text{Kr } 3d^9 5p$ configuration mainly decays to the $4p^4$ (64%) and $4s^1 4p^5$ (18%) configurations of the Kr^{2+} ion through the two-step Auger transitions. The main decay branches that reach the Kr^{2+} ion correspond to $\text{Kr } 3d^9 5p \xrightarrow{63.7\%} \text{Kr}^+ 4s^1 4p^5 5p \xrightarrow{63.6\%} \text{Kr}^{2+} 4p^4$ and $\text{Kr } 3d^9 5p \xrightarrow{18.0\%} \text{Kr}^+ 4p^5 5p \xrightarrow{18.0\%} \text{Kr}^{2+} 4s^1 4p^5$. It should be noted that the yield of the Kr^+ ions equals 18.0% (Table I) of what is within the experimental error bars [34].

The CI method is used to take into account the correlation effects in the study of cascade. The correlation effects are

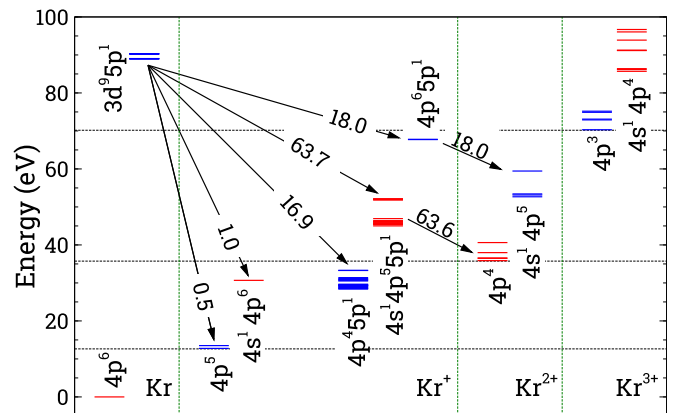


FIG. 1. Main branches of the Auger cascade for the $\text{Kr } 3d^9 5p$ configuration obtained using the single configuration calculations. Numbers at arrows mark the transfer of population in percents. The energies of the ground levels for Kr^+ , Kr^{2+} , and Kr^{3+} ions are shown by horizontal dashed lines.

TABLE I. Ion yields for the Auger cascade following the $3d \rightarrow 5p$ excitation in Kr. Expt.—experiment [34]; SC—single configuration approximation; CI_{*i*} (*i* = 1, . . . , 4)—CI for different basis sets. See text for explanation.

| Method | Kr ⁺ | Kr ²⁺ | Kr ³⁺ |
|-----------------|-----------------|------------------|------------------|
| Expt. | 17(±1) | 73(±1) | 10(±1) |
| SC | 17.8 | 82.2 | 0.0 |
| CI ₁ | 14.7 | 82.7 | 2.6 |
| CI ₂ | 13.4 | 81.0 | 5.5 |
| CI ₃ | 15.7 | 76.5 | 7.8 |
| CI ₄ | 15.7 | 76.0 | 8.3 |

studied for configurations of the Kr atom and Kr⁺, Kr²⁺, and Kr³⁺ ions. The CIS values are obtained for the configurations with the highest populations in the cascade decay, which are calculated for each set. The configurations generated using the CIS approach are also used to determine configurations in the subsequent ionization stages produced by Auger transitions from the generated ones.

Results of the ion yield (Table I) are presented for four sets of the CI bases with different numbers of the configuration state functions (CSFs). The initial study of the correlation effects (CI₁) focused on the $3d^9 4s^2 4p^6 5p$ configuration of the Kr atom. The extended CI basis was employed for these configurations, as well as for the configurations with the highest population obtained in the cascade decay, which were studied using the single configuration approximation. In addition to the $3d^9 np$ ($5 \leq n \leq 10$) and $3d^9 nf$ configurations, the $3d^9 4p^4 4d^2 5p$, $3d^9 4p^4 4d 5p 5d$, and $3d^9 4p^5 4d 5s$ configurations of the Kr atom, obtained from the CIS results, were included in the calculations. The $T/g(K)$ values are very low for these three configurations ($3d^9 4p^4 4d^2 5p$: 2×10^{-2} , $3d^9 4p^4 4d 5p 5d$: 3×10^{-3} , and $3d^9 4p^5 4d 5s$: 10^{-3}). The CI basis of the Kr⁺ ion consisted of configurations generated through Auger transitions from the configurations of the Kr atom, as well as configurations determined from the CIS calculations [$T/g(K) \gtrsim 0.1$] for Kr⁺ $4s 4p^4 4d 5p$, $4s 4p^4 5p 5d$, $4s 4p^4 5p 6d$, $4s^0 4p^4 4d^2 5p$ (admixed to $4s^0 4p^6 5p$), $4s^2 4p^3 4d 5p$, and $4s^2 4p^3 5p 5d$ (admixed to $4s 4p^5 5p$), in addition to configurations obtained from single configuration calculations of the cascade decay. Furthermore, the CI bases also included configurations produced by electric dipole transitions from the previously generated configurations. Similarly, the CI bases for the Kr²⁺ and Kr³⁺ ions were constructed in a similar manner. The CI₁ basis (Table I) consists of 17272 odd-parity CSFs of the Kr atom, 34088 odd-parity CSFs of Kr⁺, 9963 even-parity CSFs of Kr⁺, 753 odd-parity CSFs of Kr²⁺, 700 even-parity CSFs of Kr²⁺, 429 odd-parity CSFs of Kr³⁺, and 856 even-parity CSFs of Kr²⁺. The correlations effects included in the study produce yield of 2.6% for the Kr³⁺ ion (Table I).

The study primarily focused on the correlation effects in the configurations of Kr⁺, Kr²⁺, and Kr³⁺ ions in the CI₂ case. Therefore, the CI₂ set includes additional configurations for Kr⁺, Kr²⁺, and Kr³⁺ ions compared to the CI₁ set, whereas only the $3d^9 np$ and $3d^9 nf$ configurations are considered for the Kr atom. The CI basis included admixed configurations with $T/g(K)$ approximately greater

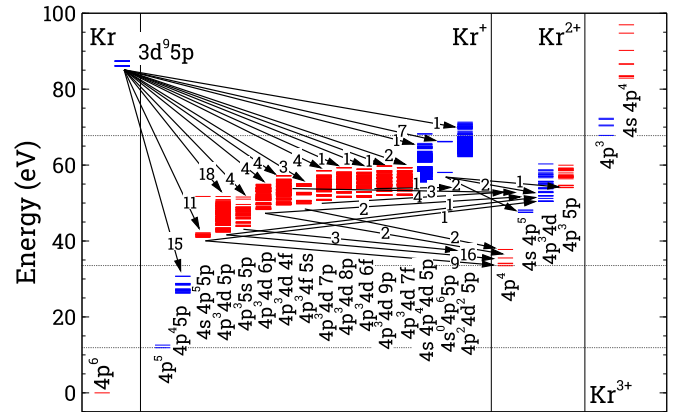


FIG. 2. Same as Fig. 1 but the CI calculations. The branches exceeding transfer of population by 1% are presented. The energies of the ground levels for Kr⁺, Kr²⁺, and Kr³⁺ ions are shown by horizontal dashed lines.

than or equal to 10^{-2} for configurations that accumulated the strongest populations of the cascade decay in the CI₁ set. The CI₂ basis (Table I) consists of 212 odd-parity CSFs of the Kr atom, 39951 odd-parity CSFs of Kr⁺, 20514 even-parity CSFs of Kr⁺, 4650 odd-parity CSFs of Kr²⁺, 2020 even-parity CSFs of Kr²⁺, 769 odd-parity CSFs of Kr³⁺, and 1777 even-parity CSFs of Kr²⁺. The population of the states of the Kr³⁺ ion increases to 5.5%.

Our code used to calculate the CIS values includes configurations generated from the considered one by taking single and double excitations up to shells with a principal quantum number of $n = 7$. The CI₃ basis was extended by including admixed configurations with excitations up to shells with $n = 15$. However, this extension was mainly applied to configurations above the single ionization threshold of the corresponding ion, which had nonzero populations resulting from cascade decay. The configurations that could lead to states of the Kr³⁺ ion were identified and, for those configurations, excitations up to shells with $n = 20$ were included in the CI₄ set.

The CI₃ basis (Table I) consists of 18804 odd-parity CSFs of the Kr atom, 59543 odd-parity CSFs of Kr⁺, 57964

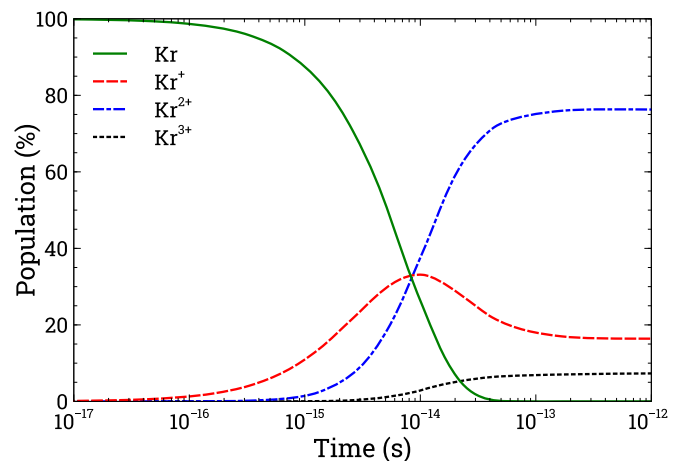


FIG. 3. Time dependence of population for the Kr atom and Kr⁺, Kr²⁺, and Kr³⁺ ions.

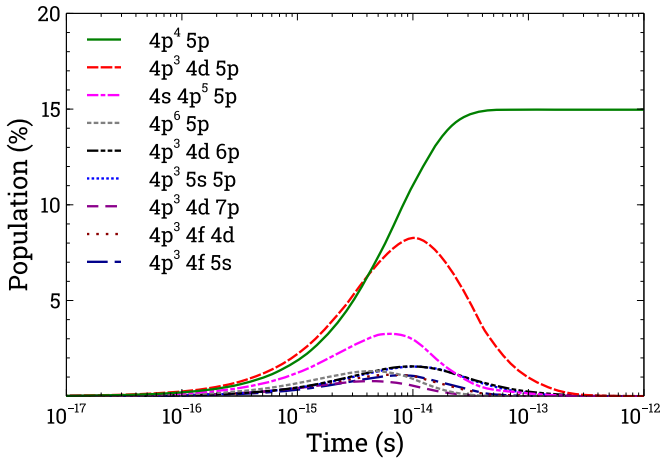


FIG. 4. Time dependence of population for the configurations of the Kr^+ ion.

even-parity CSFs of Kr^+ , 22109 odd-parity CSFs of Kr^{2+} , 17062 even-parity CSFs of Kr^{2+} , 3330 odd-parity CSFs of Kr^{3+} , and 3522 even-parity CSFs of Kr^{2+} . This case corresponds to the increase of the population by an additional 2.3% compared to the CI_2 basis.

The CI_4 basis (Table I), which is the largest one used in this work, consists of 18964 odd-parity CSFs of the Kr atom, 75789 odd-parity CSFs of Kr^+ , 57512 even-parity CSFs of Kr^+ , 22489 odd-parity CSFs of Kr^{2+} , 17382 even-parity CSFs of Kr^{2+} , 3330 odd-parity CSFs of Kr^{3+} , and 3522 even-parity CSFs of Kr^{2+} . This leads to the Kr^{3+} ion yield of 8.3%, which is in a close agreement to the measurements [34].

Table I shows that increasing the number of CSFs leads to a higher yield of the Kr^{3+} ions. It should be noted that the convergence of the data is very slow. The larger CI bases are needed to provide a better agreement to measurements. Nevertheless, obtained results show that a proper treatment of the correlation effects is a crucial factor in explaining production of the higher ionization stages in the Auger cascade. Furthermore, by this, the long-standing problem about an origin of the Kr^{3+} ion in the decay process of the $\text{Kr } 3d^9 5p$ configuration is resolved. What is more, the experimental ion

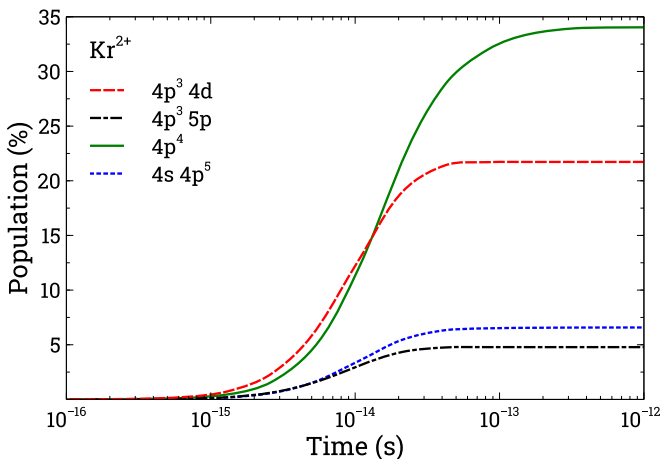


FIG. 5. Time dependence of population for the configurations of the Kr^{2+} ion.

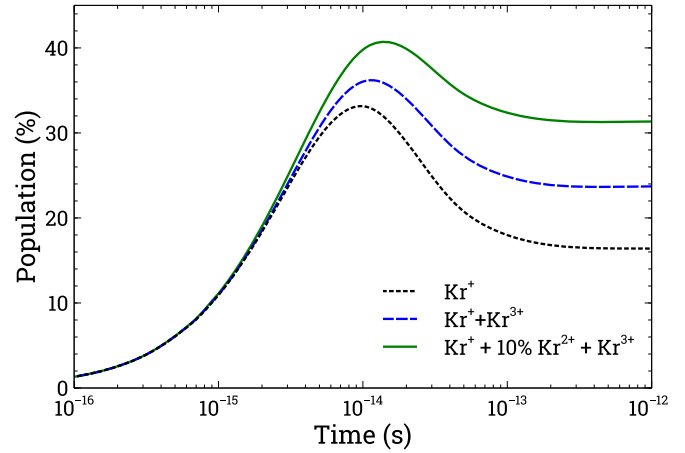


FIG. 6. Time dependence of population for Kr^{3+} , $\text{Kr}^+ + \text{Kr}^{3+}$, and $\text{Kr}^+ + 10\% \text{Kr}^{2+} + \text{Kr}^{3+}$.

yield is reproduced without making any assumptions about the contribution of the shake or higher-order Auger transitions. Previous studies associated the appearance of the Kr^{3+} ion by the triple Auger transitions [34]. The direct transitions would lead practically instantly to the states of the Kr^{3+} ion. Such effect could be detected by the pump-probe experiments when an instant emission of three electrons would be observed.

The main branches of the Auger cascade following the resonant $3d \rightarrow 5p$ excitation in Kr are shown in Fig. 2 for the largest CI basis (198989 CSFs) used in our study. It can be seen that there are no strong branches reaching the states of the Kr^{3+} ion. The number of transitions leading to the $\text{Kr}^{3+} 4s^2 4p^3$ configuration amounts to 64 in our analysis. However, the transferred population of every transition is lower than 0.6%. The $\text{Kr}^{2+} 4p^3 nl$ ($n \leq 20$, $l = 1, 2, 3$) configurations accumulate the main populations that decay to the Kr^{3+} ion. These configurations are a result of the correlation effects included in the study.

The attosecond spectroscopy showed that production of the Kr^{3+} ions increases up to ~ 7 – 15 fs of time delays for the probe pulse of the near-infrared (NIR) laser [19]. The Kr^+ ion yield later decreases and forms a flat plateau. Theoretical study of the time dependence of the population of the Kr^+ ion shows that the peak in the Auger cascade is reached at ~ 8 fs (Fig. 3). This value is in agreement with the time-dependent yield of the Kr^{3+} ion observed using attosecond spectroscopy at lower NIR intensities [$I_{\text{NIR}} = (8.6 \pm 1) \times 10^{13} \text{ W cm}^{-2}$] [19]. On the other hand, the peaks and ion yields for the Kr^{3+} ion depend on the intensity of the NIR pulse used in measurements. For the higher NIR intensities, the peak of the population for the Kr^{3+} ion leads to higher time delays between XUV and NIR pulses (~ 15 fs) [19]. However, more information about the yield of the other ions than Kr^{3+} is crucial to define which states of the Kr ions produced by the cascade are affected by the probe pulse. Furthermore, Auger spectra observed at the different time delays would provide additional information about the triggered states by the NIR pulse.

Analysis of time dependence of populations for configurations of the Kr^+ ions reveals that the $4p^3 4d 5p$ and $4s 4p^5 5p$ configurations are mainly responsible for the formation of a peak of the population for the Kr^+ ion at time delays of ~ 8 fs

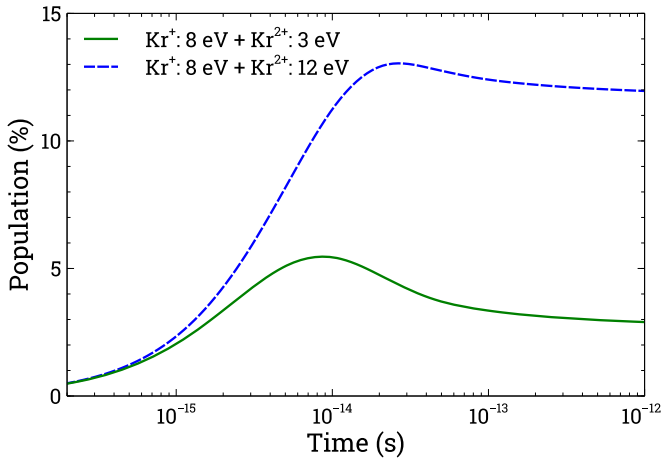


FIG. 7. Time dependence for the sum of populations of states below the ground level of the Kr^{3+} ion. Solid line: population of the states of the Kr^+ ion below by 8 eV and Kr^{2+} -3 eV; dashed line: Kr^+ -8 eV and Kr^{2+} -12 eV.

(Fig. 4). The total contribution of other configurations, which decay to Kr^{2+} , equals $\sim 5\%$ at the peak of the population. The final main population of the Kr^+ ion, which does not decay to Kr^{2+} , resides in the $4p^45p$ configuration.

There are four configurations of the Kr^{2+} ion that accumulate the final population of the ion (Fig. 5). However, this study does not include contributions from the radiative transitions since their probabilities are much lower compared to the Auger ones. The fluorescence yield of the autoionizing energy levels, determined through the cascade decay process using the single configuration approximation, is below 5×10^{-4} . Hence the impact of radiative transitions is considered negligible. The radiative transitions would change the final population of the configurations, which cannot decay through the Auger transitions. On the other hand, the inclusion of the radiative transitions would not affect the ion yields of the cascade and population dynamics.

The NIR pulse can affect not only the states of the Kr^+ ion but also the population from the Kr^{2+} ion can be transferred to the Kr^{3+} ion. To demonstrate a possible contribution of the populations from different ions, the populations of Kr^+ and Kr^{3+} are summed (Fig. 6). In addition, the populations of the Kr^+ , 10% of Kr^{2+} , and Kr^{3+} ions are summed and compared to the evolution of the population for the Kr^+ ion. It can be seen from Fig. 6 that the positions of peaks depend on the contribution of the different ions.

The probe laser pulse can reach states of various ions below the ionization thresholds and transfer populations from these

states to the higher ionization stages. The populations of the Kr^+ states, which have energies higher than energy below the ground level of the Kr^{3+} ion by 8 eV, are added to the populations of the Kr^{2+} states, which are higher than energy below the ground level of the Kr^{3+} ion by 12 eV, to demonstrate possibilities to study a contribution of the different states reached by the probe laser pulse (Fig. 7). The obtained data are compared to the case where the states of the Kr^{2+} ion with the energies higher than the energy below the ground state of the Kr^{3+} ion by 3 eV are taken. The peaks are formed at ~ 25 fs and ~ 8 fs for the presented cases. However, Auger spectra and yields of the different ions at different NIR intensities are needed to model the influence of the probe laser pulse on the populations of the states of the ions produced in the cascade decay.

IV. CONCLUSIONS

The Auger cascade following the $3d \rightarrow 5p$ excitation is investigated for the Kr atom. The long-standing problem about the origin of the Kr^{3+} ions in the Auger cascade is resolved. Systematic and large-scale CI calculations involving $\sim 200\,000$ CSFs are performed to explain the measurements. No assumptions about the shake and multiple Auger transitions in the decay process are needed to reproduce experimental ion yields. This demonstrates that a proper treatment of the correlation effects plays a crucial role in the study of the decay process. It is necessary for the CI bases to incorporate configurations that correspond to excitations to shells with high principal quantum numbers. Furthermore, when analyzing the correlation effects, careful assessment of data convergence is of great importance. Convergence of data in this study demonstrates that much larger bases of interacting configurations are needed to provide a better agreement to the experimental data for the ion yields.

The evolution of the population over time for charge states is studied. What is more, the dynamics of the Auger cascade is investigated for configurations and charge states. Analysis of a time dependence for the population of the Kr^+ ion shows a peak at ~ 8 fs, which is in a close agreement with measurements. The study shows that contribution from the other ions in the probe-pulse experiment is also possible. Modeling demonstrates that contributions of the populations from deeper states of the Kr^{2+} ion produce peaks at higher time delays compared to the energetically higher states. However, experimental data for yields of the other ions (not only Kr^{3+}) and Auger spectra are needed to estimate the influence of the probe laser pulse at the different time delays on the states of the produced ions in the Auger cascade.

- [1] C. Pinto, J. S. Kaastra, E. Costantini, and F. Verbunt, *Astron. Astrophys.* **521**, A79 (2010).
- [2] C. Pinto, J. S. Kaastra, E. Costantini, and C. de Vries, *Astron. Astrophys.* **551**, A25 (2013).
- [3] M. Rose, M. Elvis, and C. N. Tadhunter, *Mon. Not. R. Astron. Soc.* **448**, 2900 (2015).
- [4] M. Molina *et al.*, *Astrophys. J.* **922**, 155 (2021).

- [5] J. Negus *et al.*, *Astrophys. J.* **920**, 62 (2021).
- [6] A. Bartnik, P. Wachulak, H. Fiedorowicz, and W. Skrzeczanowski, *Phys. Plasmas* **23**, 043512 (2016).
- [7] G. P. Loisel, J. E. Bailey, D. A. Liedahl, C. J. Fontes, T. R. Kallman, T. Nagayama, S. B. Hansen, G. A. Rochau, R. C. Mancini, and R. W. Lee, *Phys. Rev. Lett.* **119**, 075001 (2017).
- [8] S. White *et al.*, *Phys. Rev. E* **97**, 063203 (2018).

- [9] M. E. Foord, R. F. Heeter, P. A. M. van Hoof, R. S. Thoe, H. K. Chung, D. A. Liedahl, P. T. Springer, J. E. Bailey, M. E. Cuneo, G. A. Chandler *et al.*, *Phys. Rev. Lett.* **93**, 055002 (2004).
- [10] S. Fujioka *et al.*, *Nat. Phys.* **5**, 821 (2009).
- [11] B. Rudek *et al.*, *Nat. Photon.* **6**, 858 (2012).
- [12] B. Boudaïffa *et al.*, *Science* **287**, 1658 (2000).
- [13] L. Sanche, *Nat. Mater.* **14**, 861 (2015).
- [14] A. Pronschinske *et al.*, *Nat. Mater.* **14**, 904 (2015).
- [15] G. Sgouros, L. Bodei, M. R. McDevitt, and J. R. Nedrow, *Nat. Rev. Drug Discov.* **19**, 589 (2020).
- [16] R. W. Howell, *Int. J. Radiat. Biol.* **99**, 2 (2023).
- [17] F. Calegari *et al.*, *Science* **346**, 336 (2014).
- [18] A. Sommer *et al.*, *Nature (London)* **534**, 86 (2016).
- [19] K. Hütten *et al.*, *Nat. Commun.* **9**, 719 (2018).
- [20] R. Pazourek, S. Nagele, and J. Burgdörfer, *Rev. Mod. Phys.* **87**, 765 (2015).
- [21] M. Ossiander *et al.*, *Nat. Phys.* **13**, 280 (2017).
- [22] M. Uiberacker *et al.*, *Nature (London)* **446**, 627 (2007).
- [23] B. K. McFarland *et al.*, *Nat. Commun.* **5**, 4235 (2014).
- [24] S. Kučas, A. Kynienė, Š. Masys, and V. Jonauskas, *Astron. Astrophys.* **654**, A74 (2021).
- [25] S. Kučas *et al.*, *J. Quant. Spectrosc. Radiat. Transfer* **288**, 108249 (2022).
- [26] J. Palaudoux *et al.*, *Phys. Rev. A* **82**, 043419 (2010).
- [27] A. Müller *et al.*, *Phys. Rev. Lett.* **114**, 013002 (2015).
- [28] T. A. Carlson and M. O. Krause, *Phys. Rev. Lett.* **14**, 390 (1965).
- [29] L. S. Cederbaum, J. Zobeley, and F. Tarantelli, *Phys. Rev. Lett.* **79**, 4778 (1997).
- [30] T. Hayaishi *et al.*, *J. Phys. B* **17**, 3511 (1984).
- [31] H. Aksela, S. Aksela, H. Pulkkinen, G. M. Bancroft, and K. H. Tan, *Phys. Rev. A* **33**, 3876 (1986).
- [32] E. V. Raven, M. Meyer, M. Pahler, and B. Sonntag, *J. Electron. Spectrosc. Relat. Phenom.* **52**, 677 (1990).
- [33] H. Aksela, S. Aksela, H. Pulkkinen, and A. Yagishita, *Phys. Rev. A* **40**, 6275 (1989).
- [34] P. Lablanquie and P. Morin, *J. Phys. B* **24**, 4349 (1991).
- [35] F. Zhou, Y. Ma, and Y. Qu, *Phys. Rev. A* **93**, 060501(R) (2016).
- [36] A. Müller *et al.*, *Phys. Rev. A* **97**, 013409 (2018).
- [37] V. Jonauskas and Š. Masys, *J. Quant. Spectrosc. Radiat. Transfer* **229**, 11 (2019).
- [38] T. Uphues *et al.*, *New J. Phys.* **10**, 025009 (2008).
- [39] A. J. Verhoef *et al.*, *New J. Phys.* **13**, 113003 (2011).
- [40] M. F. Gu, *Can. J. Phys.* **86**, 675 (2008).
- [41] S. Kučas, V. Jonauskas, and R. Karazija, *Phys. Scr.* **55**, 667 (1997).
- [42] V. Jonauskas, R. Karazija, and S. Kučas, *J. Phys. B* **41**, 215005 (2008).
- [43] V. Jonauskas, S. Kučas, and R. Karazija, *Phys. Rev. A* **84**, 053415 (2011).
- [44] R. Karazija and S. Kučas, *J. Quant. Spectrosc. Radiat. Transfer* **129**, 131 (2013).
- [45] R. D. Cowan, *The Theory of Atomic Structure and Spectra* (University of California Press, Berkeley, CA, 1981).
- [46] B. M. Lagutin *et al.*, *J. Phys. B: At., Mol., Opt. Phys.* **36**, 3251 (2003).
- [47] S. Kučas, R. Karazija, V. Jonauskas, and S. Aksela, *Phys. Scr.* **52**, 639 (1995).
- [48] V. Jonauskas, R. Karazija, and S. Kučas, *J. Electron. Spectrosc. Relat. Phenom.* **107**, 147 (2000).
- [49] V. Jonauskas, L. Partanen, S. Kučas, R. Karazija, M. Huttula, S. Aksela, and H. Aksela, *J. Phys. B: At., Mol., Opt. Phys.* **36**, 4403 (2003).